Progress in Oceanography 77 (2008) 351–366

Contents lists available at ScienceDirect

Progress in Oceanography

journal homepage: www.elsevier.com/locate/pocean

Observed subsurface signature of Southern Ocean sea level rise

Rosemary Morrow *, Guillaume Valladeau, Jean-Baptiste Sallee

LEGOS/OMP, 18 Av. Edouard Belin, 31401 Toulouse Cedex 9, France

ARTICLE INFO

Article history:
Received 11 September 2006
Accepted 28 March 2007
Available online 10 April 2008

Keywords:
Southern Ocean
Fronts
Sea level
Climate modes

ABSTRACT

Satellite altimetry data show a strong increase in sea level in various parts of the Southern Ocean over the 1990s. In this paper, we examine the causes of the observed sea level rise in the region south of Australia, using 13 years of repeat hydrographic data from the WOCE SR3 sections, and the SURVOSTRAL XBT and surface salinity data. The hydrographic data show a poleward shift in the position of the Subtropical and the Subantarctic Fronts over the period. In the Antarctic Zone, the Antarctic Surface Water has become warmer and fresher, and the Winter Water tongue has become warmer, fresher, thinner and shallower. Increased freshening south of the Polar Front is linked to increased precipitation over the 1990s. Temperature changes over the upper 500 m account for only part of the altimetric sea level rise. The CTD sections show that the deeper layers are also warmer and slightly saltier and the observed sea level can be explained by steric expansion over the upper 2000 m. ENSO variability impacts on the northern part of the section, and a simple Sverdrup transport model shows how large-scale changes in the wind forcing, related to the Southern Annular Mode, may contribute to the deeper warming to the south.

1. Introduction

Recent studies on global sea level rise based on Topex–Poseidon satellite altimetry data have noted a strong increase in sea level in various parts of the Southern Ocean (Fig. 1a) over the period 1993–2003 (Lombard et al., 2005; Willis et al., 2004). The dynamical processes governing the sea level rise are not well understood. Different authors have calculated the steric expansion in the upper 700 m from global in situ data (Guinehut et al., 2004; Willis et al., 2004; Ishii et al., 2006) and found that it explains only 50–60% of the observed global sea level rise (Fig. 1b). They attribute the other 40–50% to ocean mass changes.

The difference between the Topex altimetric sea level rise and the steric expansion over the upper 700 m depth is shown in Fig. 1c. The largest differences occur in the Southern Ocean. The difference is sea level rise could be due to the barotropic response to variations in the wind forcing (e.g. Vivier et al., 2005), or to warming or freshening at deeper levels.

Roemmich et al. (2007) have studied the dynamical processes which cause the strong sea level rise over the last decade in the South Pacific subtropical gyre, using altimetric data, ARGO floats and a repeat WOCE hydrographic transect along 170 W. Altimetry shows that sea level rises by 12 cm in the subtropical gyre, centred around 40 S 170 W, between 1993 and 2004. The difference map (Fig. 1c) indicates that the steric expansion in the upper 700 m explains only part of the observed signal. The analysis of subsurface hydrographic data indicates a deepening of the isopycnals to ~1800 m, and the WOCE and ARGO float trajectories confirm the gyre spin-up during the 1990s. Roemmich et al. (2007) suggest that the gyre spin-up is related to the decadal intensification of wind stress curl east of New Zealand associated with the decadal increase in the atmosphere's Southern Annular Mode (SAM).

The principal mode of atmospheric forcing in the Southern Ocean is the Southern Annular Mode. Positive values of the SAM index correspond to a poleward shift and increase in the westerly winds, which strengthens the sub-polar westerly winds and weakens the subtropical westerlies (Thompson and Wallace, 2000). A positive trend in SAM has been noted since 1979 (Thompson et al., 2000), which tend to increase the wind stress curl and Ekman pumping over the midlatitude ocean gyres, raising sea level as noted by Roemmich et al. (2007). There is also stronger upwelling at higher latitudes in the Antarctic Divergence, leading to a decrease in sea level here. Hall and Visbeck (2002) have used a coupled model to investigate the Southern Ocean's response to changes in SAM. They find that the strengthened westerlies around 60 S increase the northward Ekman transport leading to anomalous upwelling of cold water along the Antarctic margins (which decreases the sea level) and anomalous downwelling around 45 S (increasing sea level). This anomalous flow also increases the vertical tilt of the isopycnals over the Southern Ocean, so that a positive SAM is associated with a stronger Antarctic Circumpolar Current (ACC).

As well as its long-term trend, the SAM index also shows higher frequency variability including distinct interannual changes.

* Corresponding author.
E-mail address: Rosemary.Morrow@cnes.fr (R. Morrow).

0079-6611/$ - see front matter © 2008 Elsevier Ltd. All rights reserved.
doi:10.1016/j.pocean.2007.03.002

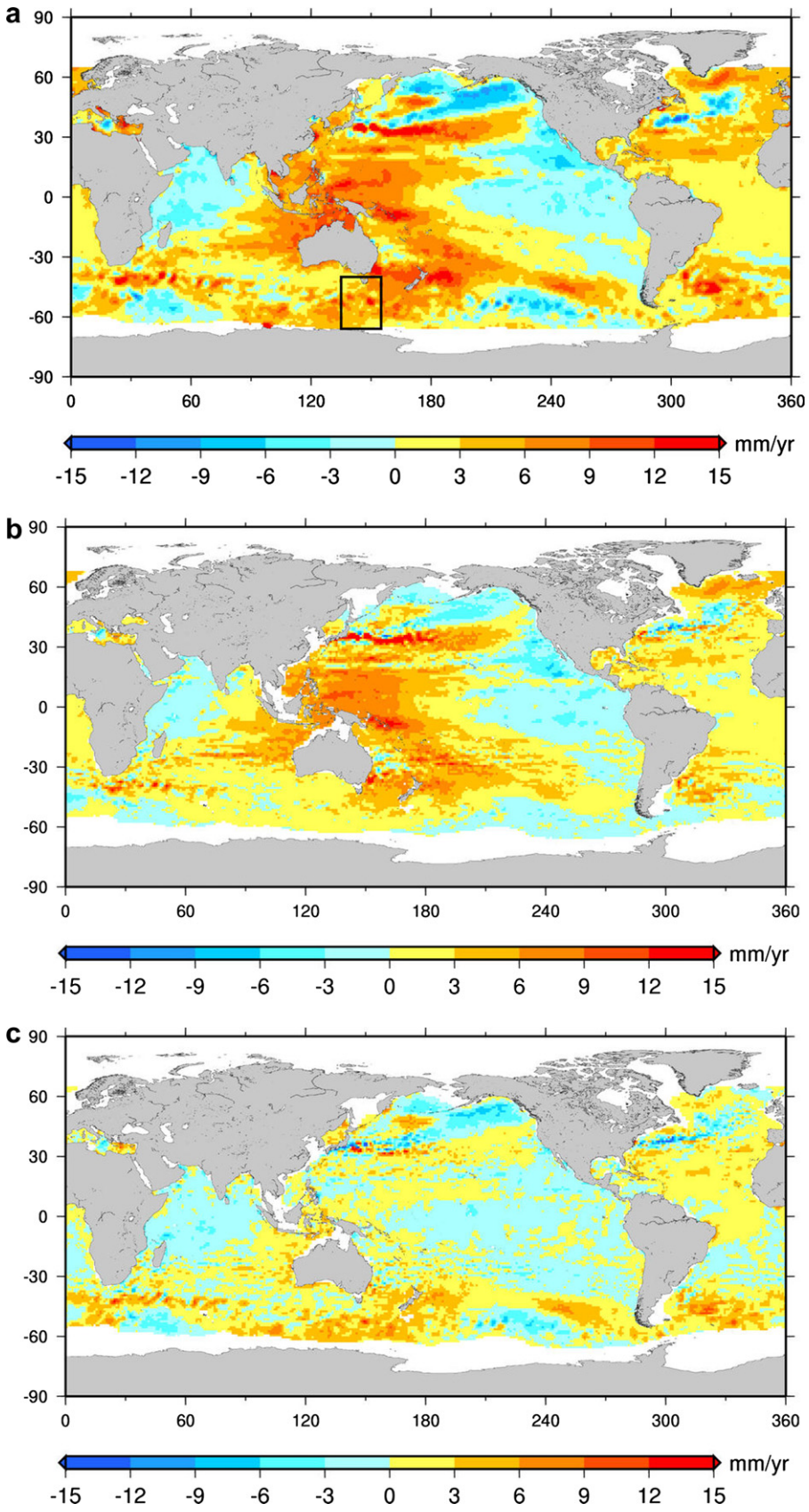

Fig. 1. Global distribution of sea level rise (in mm/year) from (top panel) Topex–Poseidon altimetric observations over 1993–2003; (middle panel) sea level rise over the upper 700 m calculated from the ARMOR in situ data projection of Guinehut et al. (2004); (bottom panel) difference map Topex – ARMOR (after Lombard et al., 2005). The study region is outlined in black.

During the 1990s, the SAM index was mainly positive with stronger events occurring during 1993–1994 and 1998–2000. After 2000, the index oscillates around zero, with two negative events occurring during 2000–2001 and 2002. These interannual changes in the strength of the SAM may also modify the strength of the convergence and divergence in the different years, leading to interannual variations in sea level.

The second mode of atmospheric variability affecting the Southern Ocean is the El Nino Southern Oscillation (ENSO). The largest impact of ENSO is predominantly felt in the South Pacific and South Atlantic (Karoly, 1989), although an oceanic response to ENSO is also noted in the SW Pacific (Holbrook and Bindoff, 1996) and in the southern Indian (Park and Gamberoni, 1995). Sallée et al. (2008) have shown that the Southern Ocean's sea level anomaly response is strongly linked to both the SAM and ENSO modes during the period 1992–2005. However, rather than a zonal response to SAM around the circumpolar belt as predicted by the coupled models, the observed sea level responds in a different way in each Southern Ocean basin. Sallée et al. (2008) found that the regional response depends on the relative strength of the ENSO and SAM modes in the different basins, the bathymetry, and the latitudinal variations in the path of the circumpolar current.

The higher latitudes of the Southern Ocean are characterised by weaker stratification and strong air–sea interactions. This means that interannual changes in the climate forcing at the surface can drive an energetic, deep-reaching thermohaline circulation (Speer et al., 2000). This will be detected by altimetric sea level observations, which respond to the vertically integrated mass and density changes. Observing and quantifying these deep ocean changes is difficult in the Southern Ocean due to the lack of long-term repeat in situ data. This situation is being improved with the vast deployment of Argo floats in the Southern Ocean since 2002 (http://www.argo.ucsd.edu). However, ARGO floats cannot solve the problem of the lack of long-term in situ observations. Two long-term monitoring sites do exist in the Southern Ocean with high-density repeat CTDs and XBTs since the 1990s: at the WOCE SR1 site in Drake Passage (Cunningham et al., 2003; Sprintall, 2003) and at the WOCE SR3 site south of Tasmania (Rintoul and Sokolov, 2001; Morrow et al., 2003).

The present paper aims to use the repeat hydrographic observations in the sector south of Australia to investigate the reasons behind the sea level rise and its interannual variations in this part of the Southern Ocean. Since 1992, in the region between Tasmania and Terre Adèlie in Antarctica, we have available concurrent high-resolution satellite altimetry and sea surface temperature (SST) data, seven WOCE SR3 repeat hydrographic transects, 76 high-resolution repeat XBT sections and 103 surface salinity sections from the SURVOSTRAL programme (Fig. 2). The satellite data and surface meteorological forcing data allows us to look at the basin-scale structure of the sea level rise and its possible forcing. The subsurface data allow us to investigate whether the surface changes are responding to variations in the surface mixed layer or to deeper temperature and salinity changes, and whether meridional frontal movements can contribute to the observed sea level rise. The relation between the SAM and ENSO climate forcing and the deeper hydrographic changes will also be explored.

2. Data sets

2.1. Altimetric sea level anomaly data

The altimeter products were produced by Ssalto/Duacs and distributed by AVISO, with support from CNES. The data set spans 12

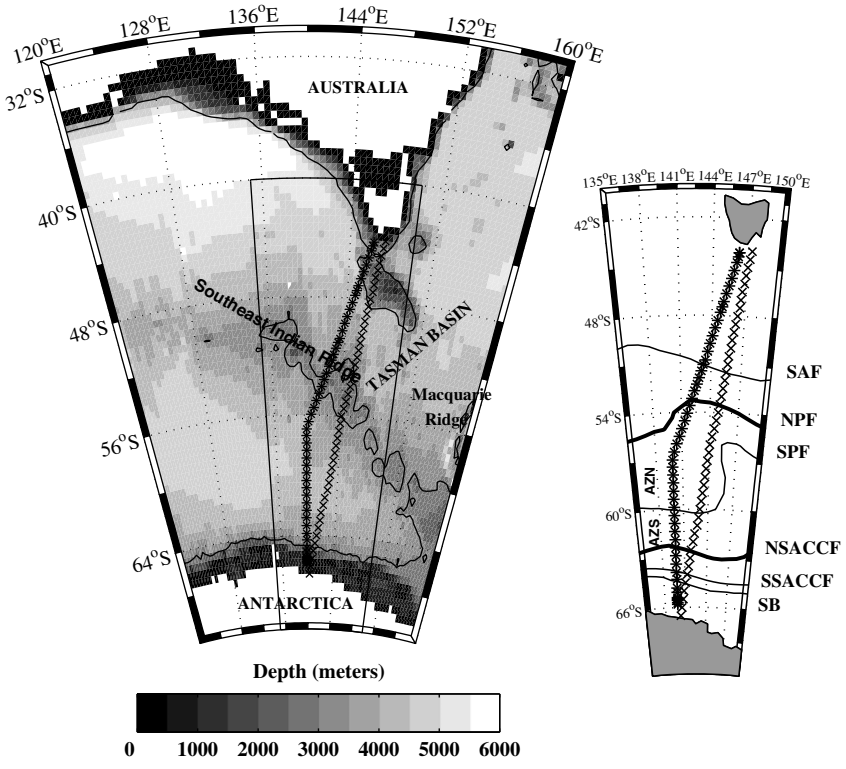

Fig. 2. (Left panel) position of the WOCE SR3 CTD transects (∗) and SURVOSTRAL XBT and TSG transects (×) between Tasmania and Antarctica, overlaid on the bathymetry. The 3000 m isobath is marked. The zoom represents the mean frontal positions defined by altimetry (Sokolov and Rintoul, 2002). The abbreviations used are: SAF, Subantarctic Front; N-PF, Northern Polar Front; S-PF, Southern Polar Front; N-SACCF and S-SACCF, Northern and Southern branch of the Southern ACC Front; SB, Southern Boundary of the ACC.

years from January 1993 to December 2004 and corresponds to sea level anomaly (SLA) relative to a seven year mean (January 1993–December 1999). Details of the mapping technique used to derive the 1/3° gridded data are given by Le Traon and Dibarboure (1999), and a discussion of the aliased high-frequency errors is given by Morrow et al. (2003). Globally, this data set resolves wavelengths greater than 150 km, with a temporal resolution of 20 days (Ducet et al., 2000). In the Southern Ocean where the groundtracks converge, we can resolve 100 km wavelengths, and variations at 50 km wavelength are present but reduced by 50% in energy.

2.2. CTD, XBT and thermosalinograph data

Five full depth repeat CTD sections are available from the WOCE (World Ocean Circulation Experiment) SR3 line, collected between Tasmania and Terre Adélie (Antarctica) during voyages of the research vessel R/V *Aurora Australis*. These sections were made in March 1993; January 1994; January 1995; July 1995; and September 1996. An additional CTD section along the SR3 line was made in November 2001 as a contribution to the CLIVAR Repeat Hydrography and Carbon Program (Rintoul and Sokolov, 2001). The station spacing for these CTD sections is around 55 km with more tightly grouped measurements in the frontal regions. The data processing steps are described in Rosenberg et al. (1995). These data are precious since they provide the only information on deep temperature and salinity changes between Australia and Antarctica over the 1990s.

As part of the SURVOSTRAL program (SURVeillance de l'Océan auSTRAL), high-density XBT and thermosalinograph measurements are obtained between Tasmania and Terre Adélie in Antarctica every austral summer. The French Antarctic supply ship "*l'Astrolabe*" was used to obtain 6 XBT and 10 thermosalinograph (TSG) sections per year along the nearly-repeating line from Hobart, Tasmania (43°S 147°E) to the French Antarctic base Dumont D'Urville (66°S, 140°E) (Fig. 2). The first XBT and TSG section for each austral summer occurs at the end of October, the final section is in mid March. The time series starts in late 1992. We are able to maintain high-density XBT sampling due to the presence of an onboard observer: weather and faulty probes permitting, XBT measurements are made every 35 km, and every 18 km in the frontal zone from 48°S to 54°S (see Fig. 2). Most observations attained 800 m depth, but nearly all reached at least 500 m. All XBT data are carefully quality controlled by the CSIRO Marine and Atmospheric Research (CMAR), Hobart, Australia. The October transects are not exactly repeating south of 60°S, as the ship searches for clear sea routes through the ice. So in the following analysis, our "summer mean" calculations are based on the available December to March exactly repeating sections.

Continuous surface temperature and surface salinity measurements are available from the thermosalinograph, with an average measurement every 1–5 min (at least one per nautical mile). Salinity data processing is described in Chaigneau and Morrow (2001).

2.3. Surface forcing data sets

2.3.1. Winds

Two different wind products will be used in the following analysis: monthly averaged winds computed from ERS gridded scatterometer winds are available on a 1.0° grid for the period 1992–1999, and higher resolution monthly Quickscat gridded winds on a 0.5° grid for the period 1999–2005. Both wind data sets are available from the IFREMER Cersat (French Satellite Processing and Archiving Facility) website (http://www.ifremer.fr/cersat).

2.3.2. Heat flux

We use the monthly NCEP reanalysis on a 2° grid to estimate the air–sea heat flux. These data are made available by the NOAA-CIRES Climate Diagnostic Center (http://www.cdc.noaa.gov/).

2.3.3. Evaporation and precipitation

Following Reverdin et al., 2007 who compared different surface forcing products in the North Atlantic, we have taken the evaporation fields from the monthly reanalysis product ERA40 of ECMWF (Simmons, A.J., Gibson, J.K., 2000, unpublished document. Available from: www.ecmwf.int/research/era). The precipitation field comes from the 1° gridded CMAP blended satellite and in situ product, available from August 2002 (Xie and Arkin, 1997).

2.3.4. Reynolds sea surface temperature

One degree resolution, weekly, optimally interpolated maps of satellite and in situ SST observations were used (http://podaac.jpl.nasa.gov/reynolds/). An analysis of this product is provided by Reynolds et al. (2002).

3. Temporal evolution of the surface characteristics

The temporal evolution in sea level rise is of course more complex than the simple trend depicted in Fig. 1a. Fig. 3a shows altimetric sea level anomalies along the SURVOSTRAL line from Tasmania (44°S) to Dumont D'Urville (66°S) from January 1993 to December 2004. The data have been low-pass filtered to remove signals less than 90 day period.

Three main zones are apparent on this map:

(1) A region of high mesoscale variability between 49°S and 54°S associated with eddies and meanders of the main dynamical fronts: the Subantarctic Front (SAF) between 49°S and 52°S and the Polar Front (PF) between 51°S and 54°S. This band is the Inter Polar Frontal Zone. Although the data have been filtered at 90-days, the annual and interannual variations of the mesoscale field are still apparent. This region shows a strong increase in sea level in 2000 and 2001 which is associated with a large increase in eddy kinetic energy (Morrow et al., 2003).
(2) North of the SAF is the Subantarctic Zone (SAZ), a region of deep winter mixed layers where Subantarctic Mode waters form (Rintoul and Trull, 2001).
(3) South of the PF is the Antarctic Zone (AZ), a region with fairly homogenous surface properties characterised by a low salinity (~33.9) due to sea ice melt and a subsurface temperature minimum layer of "Winter Water" (Chaigneau et al., 2004).

The boundaries between the different zones are delimited by the variable front positions. The SAF can be defined as the maximum temperature gradient between 3 and 8 °C at 300 m depth (Belkin and Gordon, 1996). The 3 and 8° isotherm limits are shown in bold in Fig. 3b. The maximum temperature gradient occurring within this limit is deep-reaching, and coincides with a maximum meridional sea level gradient (Sokolov and Rintoul, 2002, 2007). Recent studies have shown that the frontal positions can also be monitored using absolute sea surface height contours (Sokolov and Rintoul, 2002, 2007; Sallée et al., 2008). In the present study, we use the SAF definition of Sallée et al. (2008) (red line, Fig. 3b). This corresponds to the southern and most energetic branch of the SAF, and is defined as the 1.20 m contour of sea surface height relative to 1500 dB ($SSH_{1500\ dB}$). In Fig. 3b, we note that our SAF definition is relatively stable over time, whereas the 8 °C isotherm varies over a much larger latitudinal extent. The 8 °C isotherm is frequently pushed north of cold-core eddies which detach just north of the SAF within the SAZ (Rintoul, 1997; Morrow et al., 2004). The main frontal gradient remains to the south, as depicted by the red line.

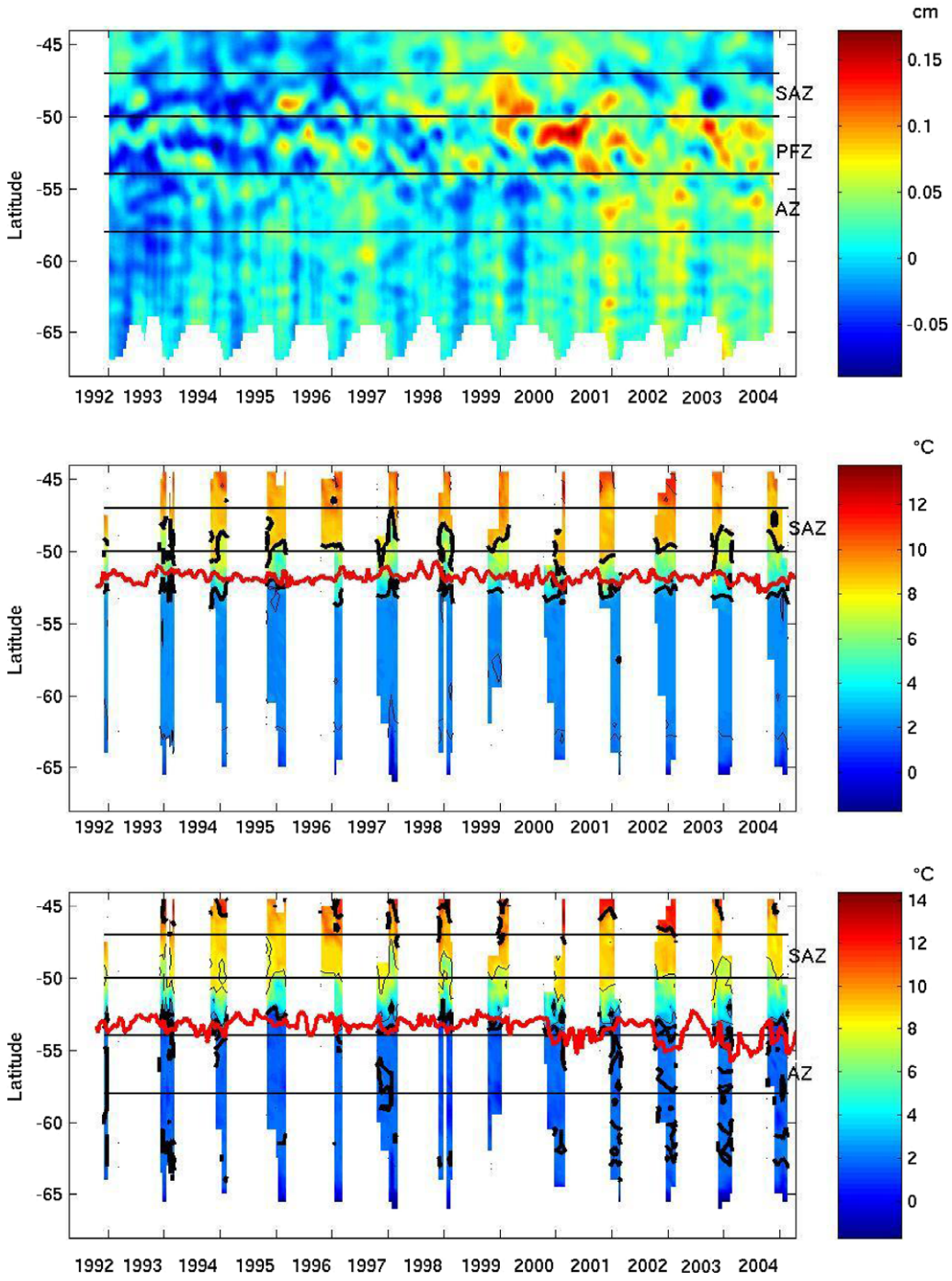

Fig. 3. (a) Hovmöller diagram of altimetric sea level anomalies along the SURVOSTRAL line from Tasmania (44°S) to Dumont D'Urville (66°S) from January 1993 to December 2004. Altimetry data are low-pass filtered to remove signals less than 90 days. (b) SURVOSTRAL XBT temperature at 300 m depth, with the 3 °C and 8 °C isotherms in bold. The SAF position is marked in red, after Sallée et al. (2008). (c) XBT temperature at 200 m depth, with the 11 °C and 2 °C isotherms in bold. The PF position from Sallée et al. (2008) is in red.

The PF is defined as the northern limit of the winter water tongue, with temperatures cooler than 2 °C at 200 m depth (Belkin and Gordon, 1996), as shown in Fig. 3c. Again, we use the Sallée et al. (2008) definition for the PF, which is the 1.0 m contour of $SSH_{1500\ dB}$, which corresponds to the northern PF position as defined by Sokolov and Rintoul (2007). We note the good correspondence between the 2 °C contour at 200 m depth and the altimetric definition of the PF in Fig. 3c.

This satellite-derived technique allows us to monitor every week the time-varying positions of the SAF and PF, and the SAZ and AZ limits, during the altimetric period 1992–2005. This is even possible for periods with no subsurface hydrographic data. In the following section, we will examine the surface forcing and the ocean response along the SURVOSTRAL line, using these variable zone limits. The SAZ is defined between 47°S and the Sallée et al. (2008) SAF position. The AZ is defined between Sallée et al. (2008) PF position and 58°S. Annual and summer means are presented where available. Summer mean values are calculated from mid December to mid March.

3.1. In the SAZ

Sea level rises to a maximum in 2000 in the SAZ (Fig. 3a, Fig. 4a), and falls thereafter in both the summer mean and annual mean values. The summer mean wind stress curl is mainly positive during the 10 year period (Fig. 4b), generating downwelling in the SAZ. The annual mean wind stress curl is near zero, strengthens to positive values in 1997–1999 and shows a larger negative anomaly in 2004. The increase in downwelling favourable annual winds during 1997–1999 precedes, and may contribute to, the peak in SLA in 2000.

The sea surface temperature (SST) and salinity (SSS) evolution is shown in Fig. 4c and e, respectively. The summer mean values of SST are from the combined SURVOSTRAL data, and the summer WOCE SR3 sections (dotted line). The summer (solid) and annual mean SST (dashed) values are also shown, based on the Reynolds SST product. The summer mean SSS values are from the TSG data and available WOCE SR3 sections. The SST and SSS values are highly correlated ($r = 0.75$), with cooler, fresher surface waters in the summers of 1993, 1998–99 and 2003–2004 with warmer, saltier waters in 2001–2002. There is no apparent correlation ($r = -0.2$) between the SST signature and the NCEP surface heat flux on a summer or annual mean (Fig. 4d), nor between the SSS signal and the biannual variations in evaporation–precipitation (E–P) data (Fig. 4f).

The periods with cooler SST in the SAZ (during 1998–1999 and 2003–2004) are periods with more summertime cold-core eddies just north of the SAF, and consistent cool temperatures over the upper 300 m (see Fig. 3b and c). If we extract the altimetric sea level anomalies at the exact space-time location as the XBT

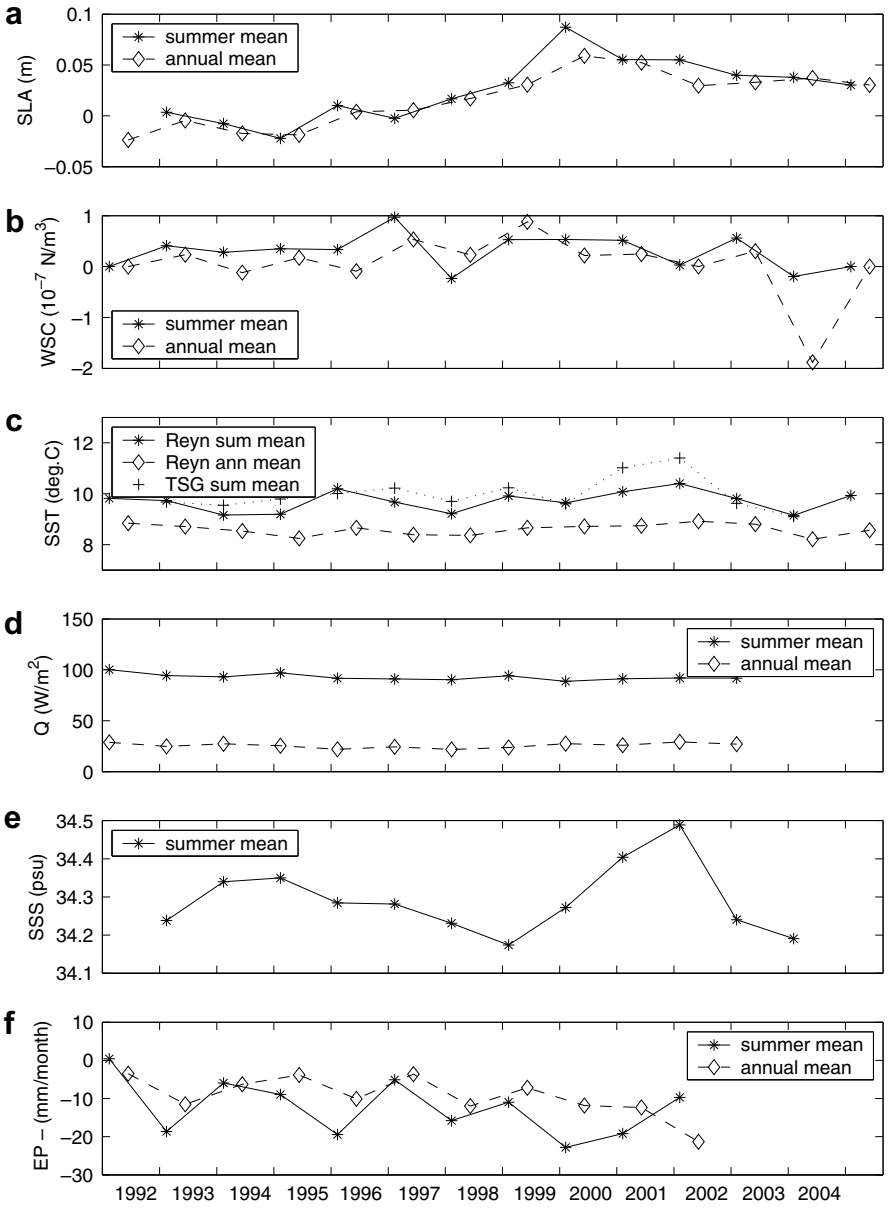

Fig. 4. Temporal evolution of the surface characteristics in the Subantarctic Zone, averaged between 47°S and the SAF position from Sallée et al. (2008), for the period 1992–2005. In all plots, the annual mean is dashed (with diamonds) and the summer mean is solid (with stars). (a) Altimetric sea level anomalies, (b) wind stress curl from the ERS and Quickscat scatterometers; (c) summer mean SST from SURVOSTRAL XBTs and WOCE SR3 summer sections (dotted). Also shown, Reynolds summer mean SST (solid), Reynolds annual mean SST (dashed). (d) NCEP surface heat flux; (e) summer mean SSS from SURVOSTRAL TSG data and WOCE SR3 summer sections; (f) surface E–P: evaporation from ECMWF and precipitation from Xie and Arkin monthly climatology.

measurements, we find a good correlation between the warm/cold eddies and positive/negative sea level anomalies, as expected. However, the summer mean averages do not always coincide, and the differences are mainly due to the in situ data sampling which is not evenly distributed each summer. For example, the peak in sea level during the summer of 2000 is due to the large positive anomaly in the north of the SAZ, which is poorly sampled by the XBTs during December 1999–January 2000. The mesoscale variations are reduced in amplitude in the summer mean calculated from the Reynolds data, and absent from the annual mean SST from Reynolds. This reinforces that the SURVOSTRAL SST and SSS data in the SAZ can be dominated by mesoscale events, such as persistent eddies or front meandering.

3.2. In the AZ

A tighter relation exists between the local atmospheric forcing and the surface characteristics in the AZ, where the mesoscale eddy energy is weaker. SLA rises over the decade (Fig. 5a), with sharper increases in 1995–1997 and 2001–2002. These interannual sea level variations appear out of phase with the SAZ, which has also been noted from a seven year time series at the same location by Sokolov and Rintoul (2003).

Although there is no net trend in wind stress curl at these latitudes, there is a weak but significant correlation ($r = 0.25$) between interannual SLA variations and local wind stress curl changes (Fig. 5b). Sea level rise occurs during periods with weaker Ekman suction. Periods of stronger Ekman suction during 1998–2000 and 2004 increases upwelling of denser water to the surface, leading to a decrease in sea level. Summer SST is also in phase with this interannual cycle in SLA and Ekman suction, and higher SLA is associated with higher SST (Fig. 5c). There is also a minor trend of increasing SST. There is no apparent interannual variation in the mean heat flux (Fig. 5d), suggesting that the SST may reflect a dynamical ocean response or remote forcing.

Interestingly, the SSS shows a net decrease of ~0.1 psu over the period, which is accompanied by an increase in precipitation of ~20 mm/month. If we assume this increase in freshwater flux is

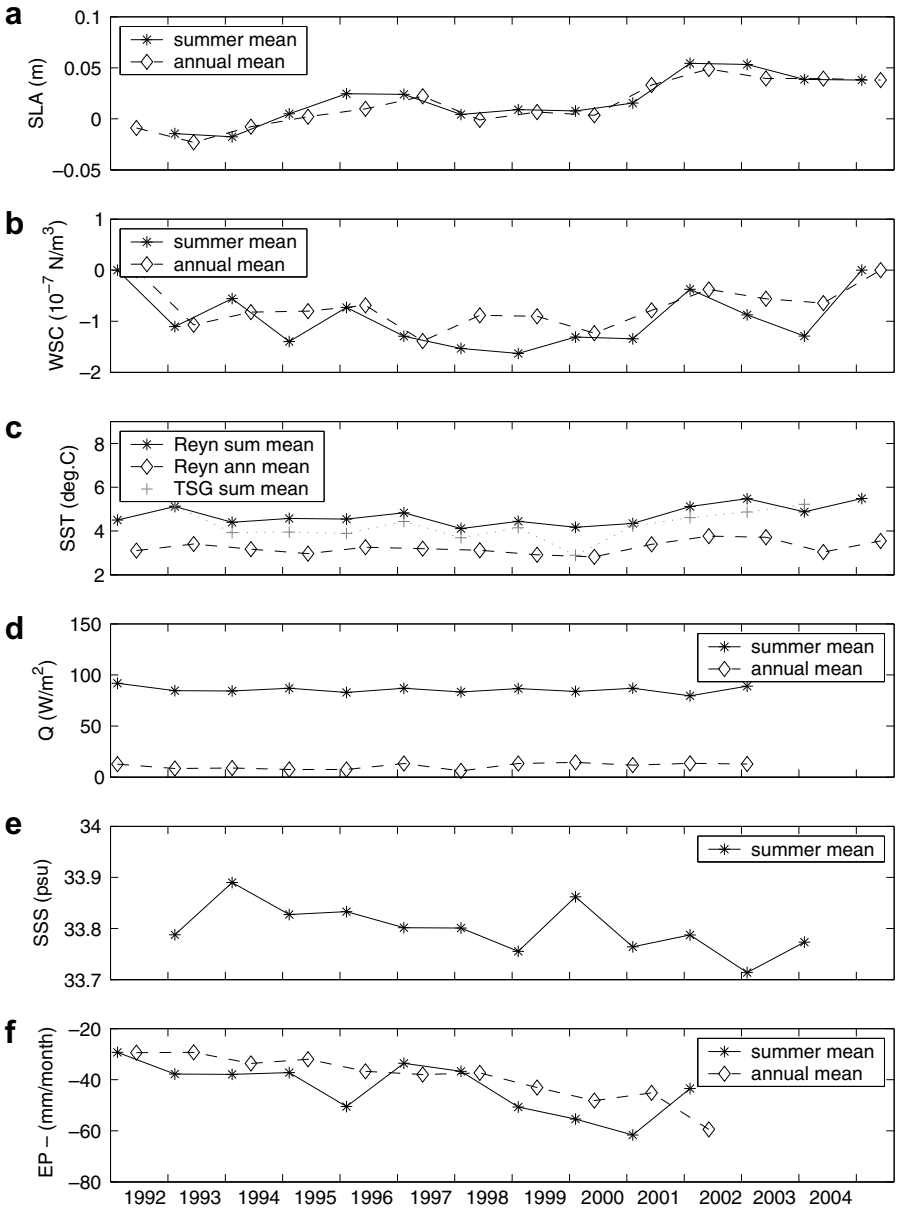

Fig. 5. As for Fig. 4, but for the Antarctic Zone averaged between the Sallée et al. (2008) PF position and 58°S.

completely mixed into the surface mixed layer (which has an average depth of 55 m in the AZ in summer, Chaigneau et al., 2004), then the precipitation increase is sufficient to explain the drop in salinity.

4. Subsurface structure

WOCE SR3 subsurface temperature and salinity data are available over the entire water column and will be used to provide information on the deep temperature and salinity changes over the 1990s. However, we will start by an analysis of the summer mean SURVOSTRAL repeat XBT data from mid December to mid March, which are statistically more robust with 4–6 sections per year over the 13 years.

4.1. XBT temperature structure in the SAZ

Sokolov and Rintoul (2003) have shown that there is a strong temperature correlation over the upper 500 m in the SAZ due to the deep winter mixed layers and the fact that the region is often subject to deep-reaching meandering fronts and detached eddies. We can see the impact of these deep-reaching mesoscale eddies and meanders when we plot the temporal evolution of the summer temperature structure at different depths in the SAZ (Fig. 6). From the surface down to 500 m depth, the summer temperature structure shows evidence of heaving isotherms which are coherent over the upper 500 m, this heaving occurs even within one summer period (e.g. January 1998). Part of the interannual change is due to the XBT sampling, with incomplete coverage in the SAZ during the summers of 1998, 2000 and 2001. Despite these sampling anomalies, there is also a background trend with temperatures increasing over the upper 400 m. The maximum increase occurs at 80 m with 0.047 °C per year, yielding a 0.6 °C temperature increase over the 13 years at this level. We note that the error bars on the trend calculation are large, due to the strong mesoscale signal in our summer observations, and only the trend at 80 m depth is statistically significant.

The background trend over the upper 500 m is equivalent to a 0.02 °C increase per year, leading to a steric sea level rise of 1.6 mm/year (assuming a constant salinity of 34.5 over the upper ocean). This is in the right sense to explain the SL rise in the SAZ but explains only one-third of the total observed sea level rise of 5 mm/year from 1993 to 2003 (Figs. 1a and 4a).

4.2. XBT temperature structure in the AZ

Fig. 7 shows the summer mean temperature evolution in the AZ, along different depth levels from 0 to 500 m depth for the period 1992–2004. Linear temperature trends are superimposed at each depth level. During this period of decadal sea level rise, temperatures increase in the surface summer mixed layer (0–40 m depth) by 0.8 °C over 12 years. Below the summer mixed layer we have the "Winter Water" (WW) layer characterised by a tongue of low temperature water <2 °C. Within this winter water layer, temperatures show a slight decrease from 80 to 120 m, and then increase again from 150 to 250 m depth. Below 300 m we are in the upper circumpolar deep water layer, and the temperatures show minor warming to ~400 m depth then cooling by <0.05° in the deepest layers. The warming trend in the surface mixed layer, and at 150 m depth is statistically significant, although the smaller temperature changes in the winter water layer and deeper than 250 m are not significant with the precision and sampling of the XBT data.

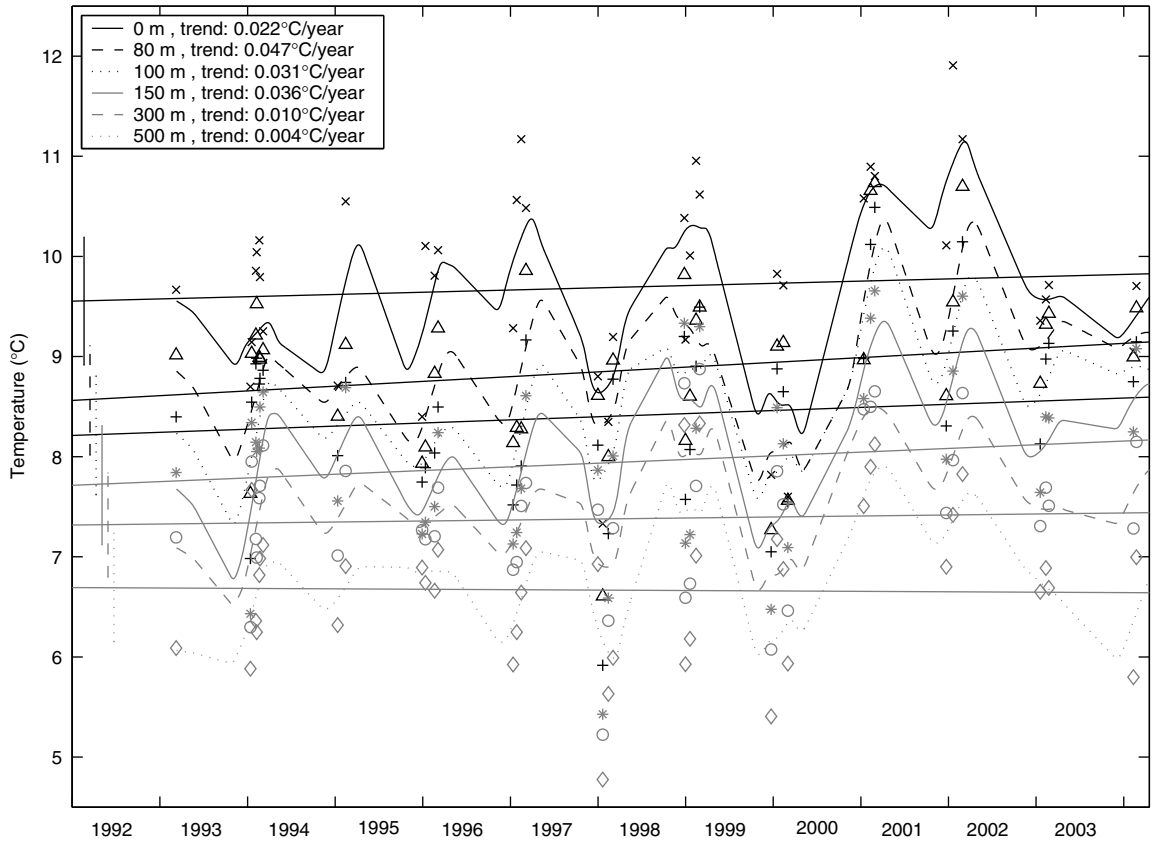

Fig. 6. Temperature trends in the SAZ, with a linear fit to the summer mean temperature data, along different depth levels from 0 to 500 m depth for the period 1992–2004.

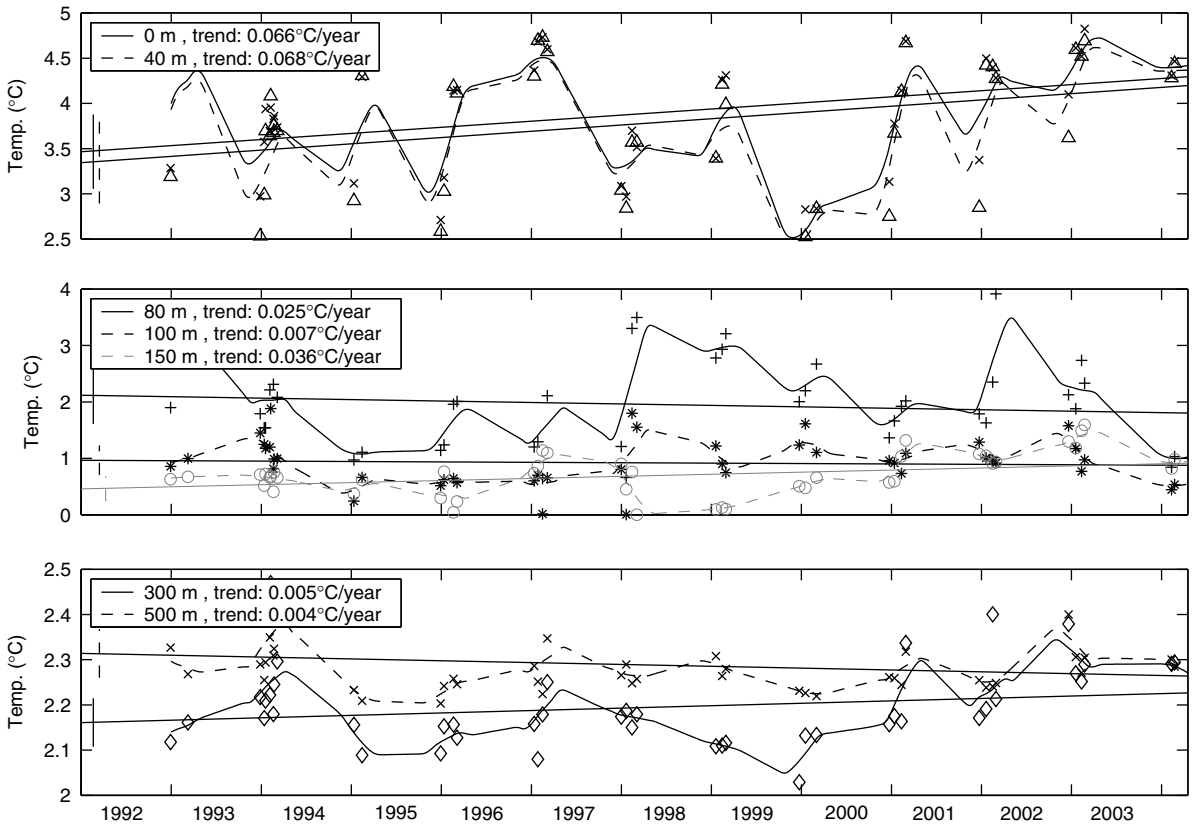

Fig. 7. Temperature trends (°C/year) in the AZ, with a linear fit to the summer mean temperature data, along different depth levels from 0 to 500 m depth for the period 1992–2004. (Top panel) temperature in the summer mixed layer from 0 to 50 m depth; (second panel) winter water layer from 80 to 250 m depth; (third panel) deep water layer from 300 to 500 m depth.

The temperature signals at 80 m and 150 m depth are mostly out of phase. The large increase in temperatures at 80 m in January 1998 is accompanied by a rapid drop in temperature at 150 m depth, whereas the temperature difference is minimal around January 2001. A large temperature gradient occurs between 80 and 150 m depth when there is a thinner core winter water layer, and vice versa.

This vision of alternative layers warming and cooling can be more clearly explained if we consider how the mean temperature structure over the section has changed between the later high sea level years (2000–2004) and the earlier years (1992–1996). Fig. 8 shows the mean temperature structure averaged (a) over 1992–1996, (b) over 2000–2004 and (c) their difference. Firstly we note that the STF, which is defined as the position of the 11 °C isotherm at 150 m depth (Nagata et al., 1988) has shifted southward from 46°S to 47°S during this period, introducing a large warming over the upper 500 m in the northern part of the section. Similarly, the northern branch of the SAF has also shifted southward from 50.5°S to 51.5°S again introducing a warming to depths greater than 500 m. So part of the observed warming and sea level rise in the SAZ may be due to a southward shift in these fronts. The southward shift in the PF has also been observed at this location by Sallée et al. (2008) in a circumpolar analysis of the frontal positions (Fig. 3c).

In the AZ the story is more complicated. There is indeed net warming in the surface mixed layer, and we have seen from the SSS data that this is accompanied by a net freshening. It is therefore unlikely that this layer is influenced by a stronger Ekman transport which would bring a larger volume of fresher but cooler water from the south. The summer wind stress curl is slightly stronger during 2000–2004 than during 1992–1996, which should introduce cooler water into the surface layer. In the absence of a net heat flux trend, the reason for the surface heating in the mixed layer is not yet understood.

The subsurface cooling and warming may be explained by the fact that the tongue of Winter Water is shallower and not as thick at the end of the period. This shift to shallower levels has the effect of cooling the layers from 80 to 120 m on the top of the tongue, and warming the layers from 150 to 250 m at the base of the tongue, although we note that only the deeper warming is statistically significant. The reason for the shallower winter water tongue may be twofold. Firstly, both the summer mean and the annual mean SST have warmed between the two periods, meaning warmer winter conditions which could reduce the winter mixed layer depth. The stronger Ekman suction in summer at the end of the period (2000, 2001 and 2004) may also "lift" the winter water tongue. Finally, close to the Antarctic continent, we also observe a net cooling by nearly 1 °C as the Southern Boundary front appears to have shifted northward, perhaps as a response to stronger upwelling along the Antarctic Continent.

4.3. CTD T–S structure

The adjacent WOCE SR3 CTD data provides valuable information on the deeper water mass changes, including the salinity changes. However, we have fewer sections available. It is a delicate task to interpret net T–S changes over a decadal period based on a limited number of sections, when seasonal modifications in the surface mixed layer and the strong mesoscale eddy signal can have a big impact on the observed variations. Bearing this in mind, we have averaged together the three summer CTD sections available in the 1992–1996 period (March 1993, January 1994, January

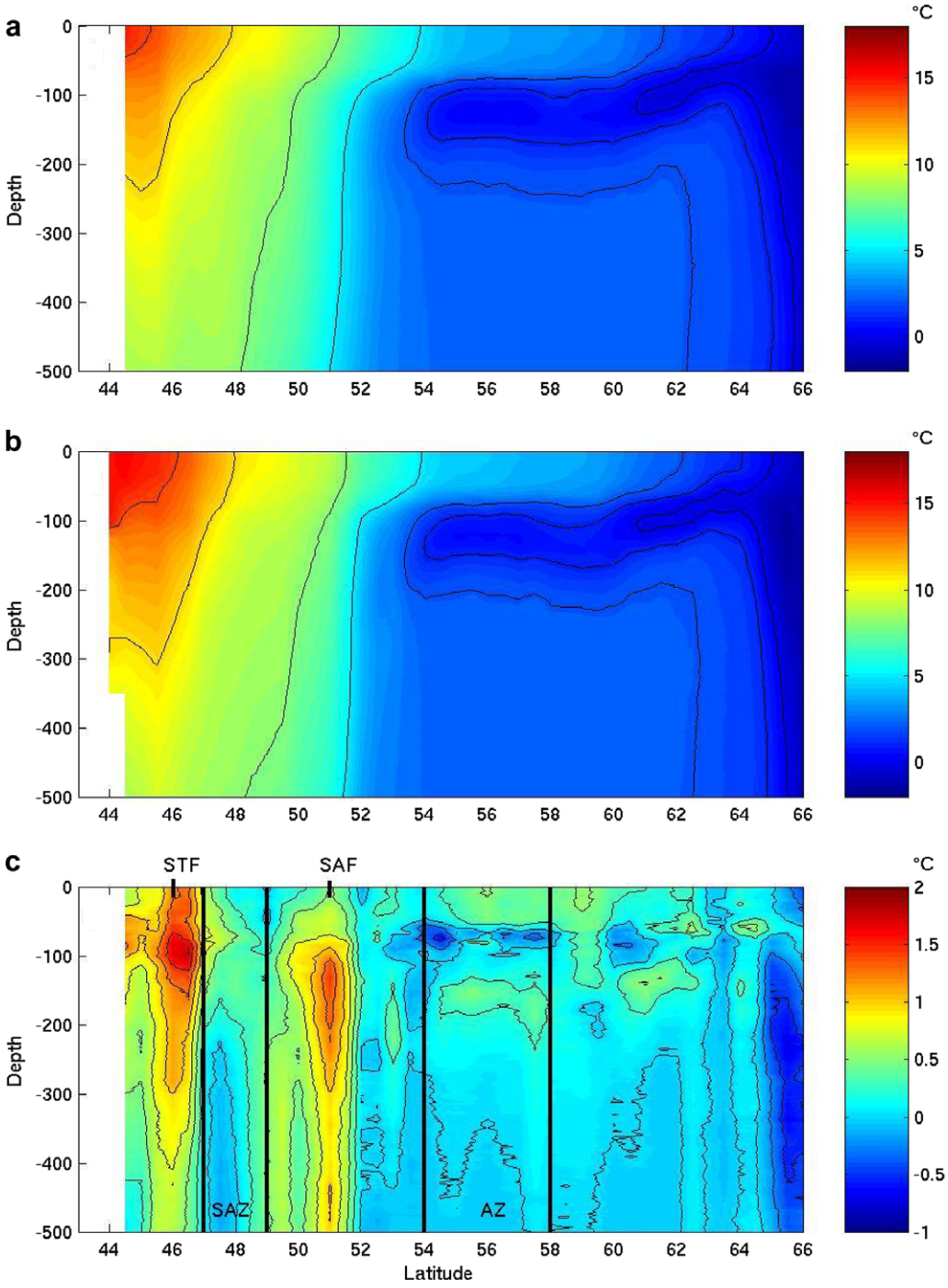

Fig. 8. Mean XBT temperature structure over 0–500 m depth averaged over the summertime SURVOSTRAL sections for the period (a) 1992–1996, (b) 2000–2004 and (c) the temperature difference between these two mean summer periods. The SAZ and AZ discussed in the text are delimited by the vertical black lines. The position of the STF and SAF are marked.

1995), and compared this summer mean to the only transect available in the period 2000–2004 (November 2001).

Fig. 9 shows the evolution of temperature and salinity from these four WOCE SR3 sections calculated in a similar way to Fig. 8. The CTD section of November 2001 shows strong mesoscale eddy structures, including a very strong cold-core eddy at 49.5°S which completely perturbs the mean position of the SAF. Despite this, the CTD difference maps (Fig. 9c) show similar features to the better-sampled XBT difference maps (Fig. 8c). There is a clear southward shift in the STF, with maximum amplitude near 100–200 m depth which tapers away near 500 m depth. The CTD sections reveal that there is additional subsurface warming between 700 and 1300 m, and the water is also saltier over the upper 1500 m. This suggests a southward meander or shift of the STF, probably associated with an increase in the Tasman Sea outflow, which brings with it warmer, saltier Tasman Sea waters over the upper 1500 m (Rintoul and Sokolov, 2001). This replaces the cooler, lower salinity mode and intermediate waters which extended north of 46°S during the early 1990s (Fig. 9a).

Altimetry maps confirm the presence of two cold-core eddies at 47°S and 49°S in November 2001; the CTD sections show these eddies have cooler water over the upper 1500 m which is fresher

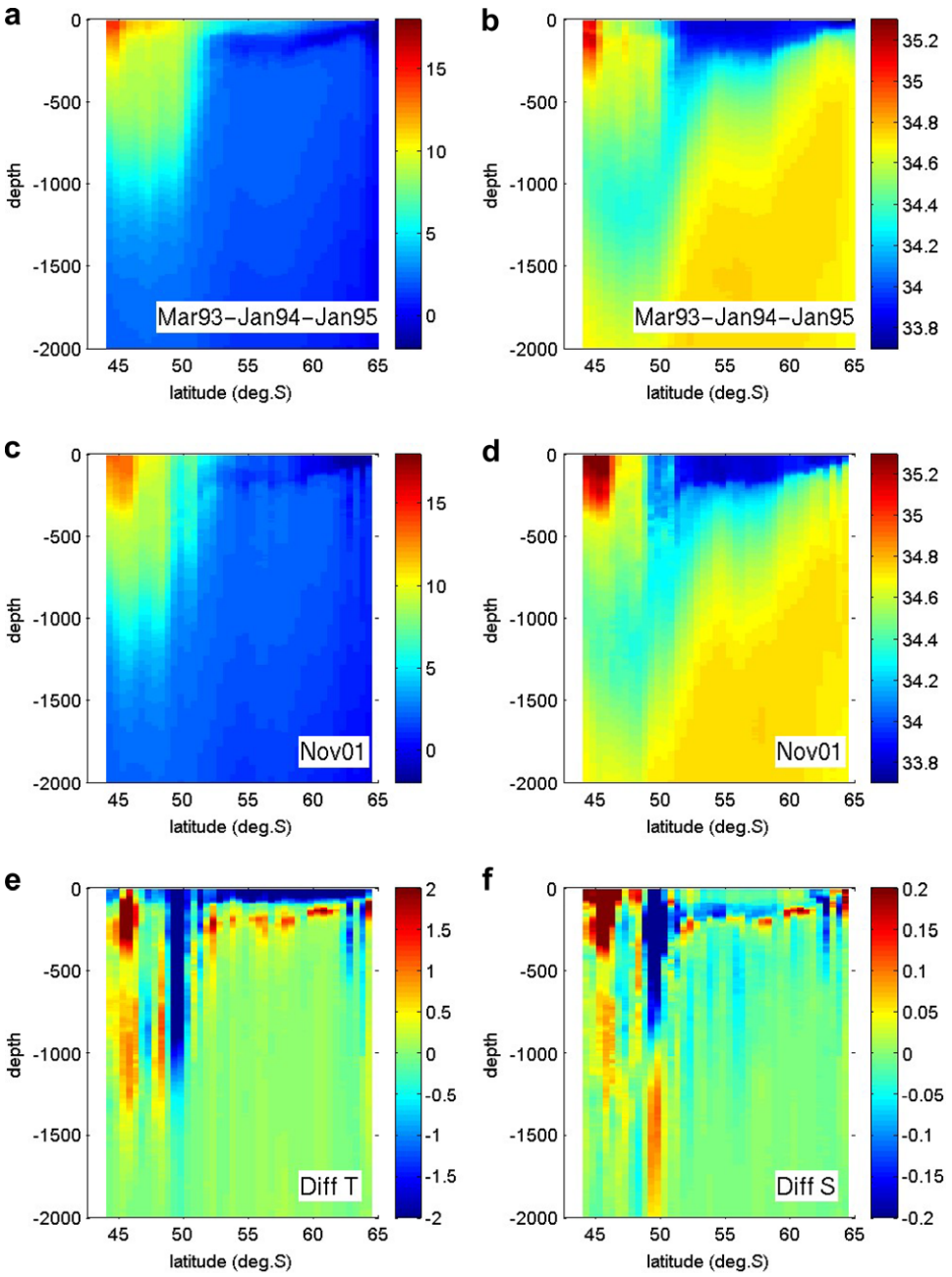

Fig. 9. Left panels: (a) mean CTD temperature structure over 0–2000 m depth averaged over the summertime WOCE SR3 sections of March 1993, January 1994, January 1995, (b) temperature structure for the November 2001 section (c) the temperature difference between these two periods. Right panels: same for salinity.

than the surrounding waters in the upper 1000 m, and saltier from 1000 to 2000 m depth. This T–S structure is characteristic of the water mass structure south of the SAF (Fig. 9). The detachment of cyclonic eddies from the SAF, transporting Polar Frontal Zone waters into the SAZ south of Tasmania, has been documented by Morrow et al. (2004).

The surface mixed layer shows cooling in the CTD difference maps whereas the XBT difference maps show a net warming. This is because we are comparing different seasons. The November 2001 section is in late spring at the start of the summer heating cycle, and the seasonal warming is only just reaching 58°S. This seasonal heating cycle is much stronger than the trend in surface temperature. The surface mixed layer extends down to ~100 m depth in the AZ in the November 2001 section.

The CTD sections do help us understand the dynamics of the evolving Winter Water tongue in the AZ. The CTD sections confirm that the Winter Water tongue appears to have diminished. The low salinity surface water still extends down to ~200 m depth in the AZ, but the water between 100 and 200 m depth shows a warmer band; as seen in the XBT profiles. This follows the tendency towards warmer, fresher winter conditions suggested earlier. There is a pronounced mesoscale signal in the AZ, evident in the November 2001 section. Warm anomalies, for example at 56°S, heave the isotherms and isohalines downward, inducing warm fresh anomalies from 300 to 1000 m depth. At the base of the winter water layer near 200 m depth there are patches of warmer, higher salinity waters where the winter water layer thickness has been locally reduced.

We have also repeated our difference calculation on isopycnal surfaces to separate the effects of eddy "heaving" from real warming/freshening at depth. In the AZ, the same structure of subsurface warming is present, although on isopycnal surfaces the anomalies

are warmer and slightly saltier. The southward movement of the STF remains both warmer and saltier. The strong subsurface warming at the base of the Winter Water tongue and lesser warming extending down to 1500–2000 m are also present in the winter SR3 sections made during August 1995 and September 1996 (not shown).

The CTD sections allow us to make more precise estimates of the steric height changes across the ACC during this period. Fig. 10 shows the steric height calculated from the mean 1993–1995 summer period, the November 2001 section, and their difference. Steric height is calculated over the upper 500 dB, similar to the XBT data analysis, and also relative to 2000 dB. The mesoscale structure, in particular from November 2001, is evident in the difference plot. Despite this, there is a net increase in the 0/2000 dB steric height in the AZ between 54°S and 63°S of 1–4 cm. Leaving aside the two cyclonic eddies in the SAZ, the southward movement of the STF also increases 0/2000 dB steric height by ~4–5 cm.

Unfortunately, November 2001 was an anomalous month in the AZ. Fig. 3a shows the temporal evolution of altimetric SLA at SURVOSTRAL, just downstream of the SR3 line, and we note the strong mesoscale activity in the AZ during November 2001. Given the strong mesoscale positive sea level anomalies, it is difficult to draw firm conclusions on the net sea level rise over the period using these four CTD sections. However, the CTD sections clearly show that the warming is not limited to the upper 700 m, and deeper warming does occur down to 1500–2000 m depth. This deep warming increases the steric height rise over 0/2000 dB by a factor of 2–3, compared with the steric height calculated from 0/500 dB. This reinforces that the steric height estimates calculated over 0/700 dB for the global sea level rise studies (Lombard et al., 2005; Willis et al., 2004; Ishii et al., 2006) will be underestimating the real steric sea level rise by at least a factor of 2–3 in this part of the Southern Ocean.

5. Relation with climate mode forcing: ENSO and SAM

How might changes in the atmospheric forcing contribute to the observed sea level rise? The two main climate modes which effect the ocean circulation south of Tasmania are the Southern Annular Mode (SAM) and the El Niño Southern Oscillation (ENSO). Fig. 11a shows the MEI ENSO Index based on a weighted average of the main ENSO features (for details see http://www.cdc.noaa.gov/ENSO/enso.mei_index.html). Positive values of the MEI Index represent the El Niño phase of ENSO, with warming in the central and eastern Pacific, and cool and dry conditions in the western Pacific. Although ENSO is a tropical coupled system, its impact can be felt in the entire southwest Pacific, carried by the East Australian Current (Holbrook and Bindoff, 1996). In our study region, the positive MEI ENSO index during 1997 corresponds to cooler ocean conditions in the South Tasman Sea, the negative MEI index corresponds to warming, which occurs during the austral summers of 1996–1997 and 1999–2000.

The Southern Annular Mode (SAM) is defined as the leading principal component of the 850 mb height anomaly in the region south of 20°S (Thompson and Wallace, 2000). The SAM index is shown for the period 1992–2005 in Fig. 11b, with a three month running average applied. The SAM has been essentially positive during the 1990s, with stronger events during in 1993, 1998–1999, and 2001. The SAM had more negative events in the 2000s, with negative indices during 2000 and 2002–2003.

Studies over the circumpolar region have found that the ENSO and SAM indices are often anti-correlated (L'Heureux and Thompson, 2005). This is certainly the case for the strong 1999 La Nina event (Fig. 11). When negative ENSO is associated with a positive SAM index, there is also a southward shift in the winds and in the position of zero wind stress curl. Rintoul and Sokolov (2001) have demonstrated that a poleward shift in the zero wind stress curl is associated with a stronger Tasman outflow, bringing

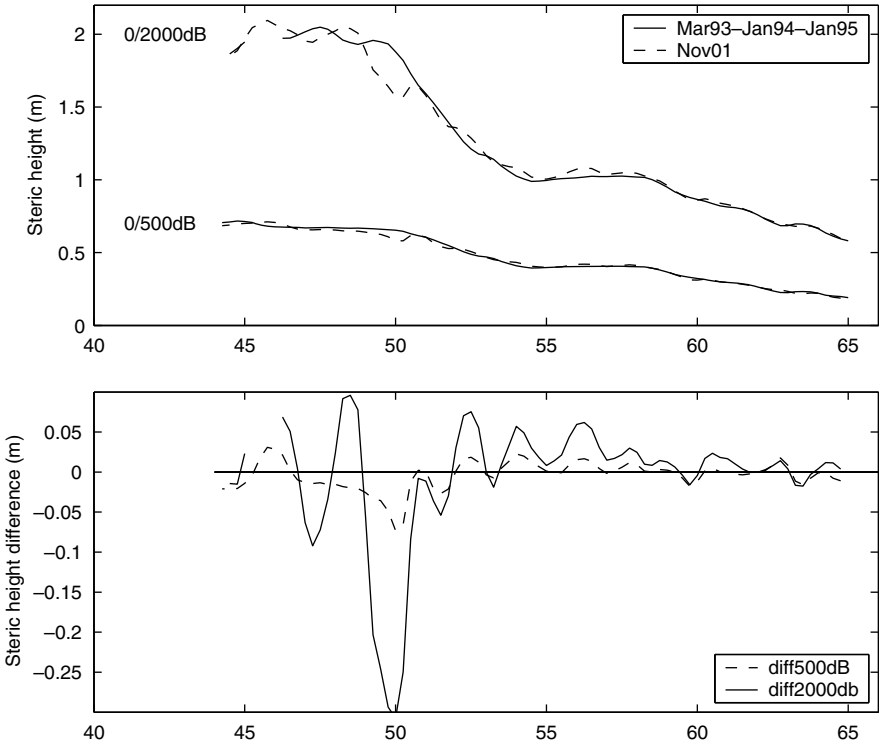

Fig. 10. (a) Steric height calculated from 0/500 dB and 0/2000 dB based on the mean of the WOCE SR3 CTD sections from March 1993, January 1994, and January 1995, and compared to the November 2001 section. (b) Steric height difference (November 2001 – Mean 93-94-95) from 0/500 dB and 0/2000 dB.

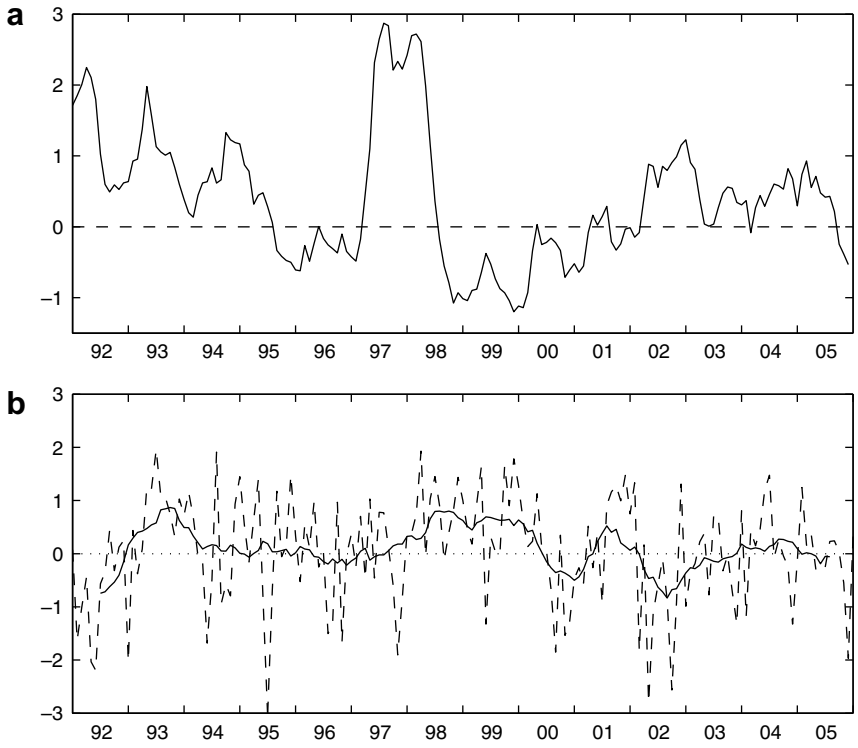

Fig. 11. Temporal evolution of the (a) MEI ENSO index, based on a weighted average of the main ENSO features and (b) the SAM index, for the period 1992–2005.

warmer, saltier water into the northern part of the section. This would increase the sea level, as observed in 1999–2000.

We have regressed the SAM index and the ENSO index onto altimetric sea level anomalies in the Southern Ocean (Fig. 12). Negative ENSO events lead to a positive sea level rise in the SAZ, with a lesser impact in the AZ south of the Polar Front. Positive SAM events during the 1990s increased downwelling in the SAZ which increased sea level, whereas there was stronger upwelling in the Antarctic divergence which tends to decrease sea level in the AZ. After 2000, when the SAM index becomes negative, the reverse occurs, with sea level falling in the SAZ and increasing in the AZ. Sallée et al. (2008) find that in the sector south of Australia, ENSO dominates the sea level response north of the SAF, and SAM dominates south of the SAF.

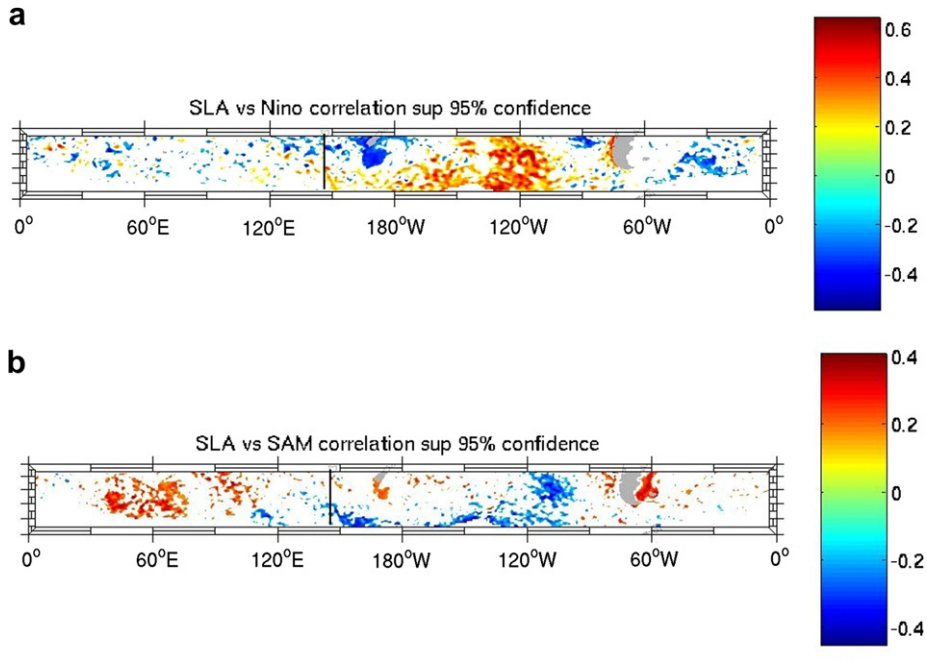

Fig. 12. Altimetric SLA regressed onto (a) the ENSO index and (b) the SAM index for the period 1993–2005 in the Southern Ocean. Only values greater than the 95% confidence level are shown. The approximate position of the SURVOSTRAL measurements is shown by the bold line.

Consider the impact of these two climate modes in the SAZ. The SAM tendency for sea level rise during the 1990s and a weak decrease after 2000 is evident in the sea level anomaly and SST fields (Fig. 4a and c). In addition, the positive ENSO forcing tends to reduce the sea level at the beginning and end of the 13 year period, and enhances the sea level rise during 1999–2000. Interestingly, the strong positive El Nino event of 1997–1998 is associated with weaker subsurface temperatures (Fig. 6) and a northward movement of the 8 °C isotherm at 300 m depth around the dominant cold-core eddies (Fig. 3b), with a minor drop in SST (Fig. 4c), but no influence on the mean SAZ sea level (Figs. 3a and 4a). It is possible that the shift to a strong positive SAM index during this period may counteract the negative sea level anomalies induced by the El Nino signal. The interplay between the ENSO and SAM forcing, and its impact on the SAZ sea level, merits further study. Unfortunately, the strong mesoscale eddy signal, particularly in the period 1998–2000, confuses the climate mode response.

In the AZ where the SAM forcing dominates, positive SAM events during the 1990s are associated with stronger negative wind stress curl (upwelling – Fig. 5b) which effectively reduces the sea level during these years, with increasing sea level during the negative SAM years 2000–2003.

Although direct SAM forcing, shifting the wind stress curl field, has an impact on the observed interannual sea level changes, there is only a weak trend in wind stress curl over the period 1992–2005 (Fig. 4b), yet there is a strong sea level rise. Why is this so? If we consider the integrated response of the wind forcing we get a more complete picture. We have calculated the Sverdrup transport based on the mean satellite winds of ERS-1 (1991–1995) and Quikscat (1999–2005), integrated over the Southern Ocean basins deeper than 2000 m. Our model integrates the wind stress curl from east to west, starting from the 2000 m depth contour along an eastern continental boundary or submerged ridge (black points), up to the western boundary (red points). Fig. 13 shows the integrated Sverdrup transport for the ERS period (top panel) and the Quikscat period (bottom panel), with a zoom over our region 70°–170°E. In the northern section of our zoom, the eastern boundary is along the New Zealand – Campbell Plateau or the coast of Tasmania. South of 55°S, the eastern boundary lies along the Falkland Ridge east of Drake Passage, or the Antarctic Peninsula further south.

During the ERS period (1991–1995) when the SAM index is mostly positive (Fig. 11b), there is an intense eastward circulation around 60°S imposed by the poleward shift and intensification of the westerly winds. There is also a noticeable westward current along the Antarctic continent. This forms a cyclonic recirculation gyre, including a westward coastal current, and an eastward recirculation further north. A much weaker cyclonic gyre has been observed with CTD sections, ADCP currents and floating buoys during the BROKE campaign in the summer of 1996 (Bindoff et al., 2000) – a period when the SAM index was close to zero. Clearly during most of the 1990s, this cyclonic gyre is more intense, implying a lower sea level. More importantly, the western boundary of this basin lies along the Kerguelen Plateau around 80°E, and this cyclonic recirculation draws in cold, fresh Antarctic Slope Current waters into the northward flowing western boundary current (Bindoff et al., 2000; Speer and Forbes, 1994). Part of this flow originates in the Weddell–Enderby Basin, passing south of the Kerguelen Plateau via the Princess Elizabeth Trough (Wong et al., 1998). These cool, fresh western boundary current waters are then transported eastward from 55°S to 60°S by the integrated Sverdrup flow in the upper 2000 m (Fig. 13). Numerical model results suggest that thes waters reach the SURVOSTRAL line some 12–18 months later (Speich, S., personal communication). Stronger cool-fresh flow implies a lower sea level in the early 1990s.

During the Quikscat period (1999–2005) when more negative SAM events occurred, the integrated Sverdrup flow has weakened

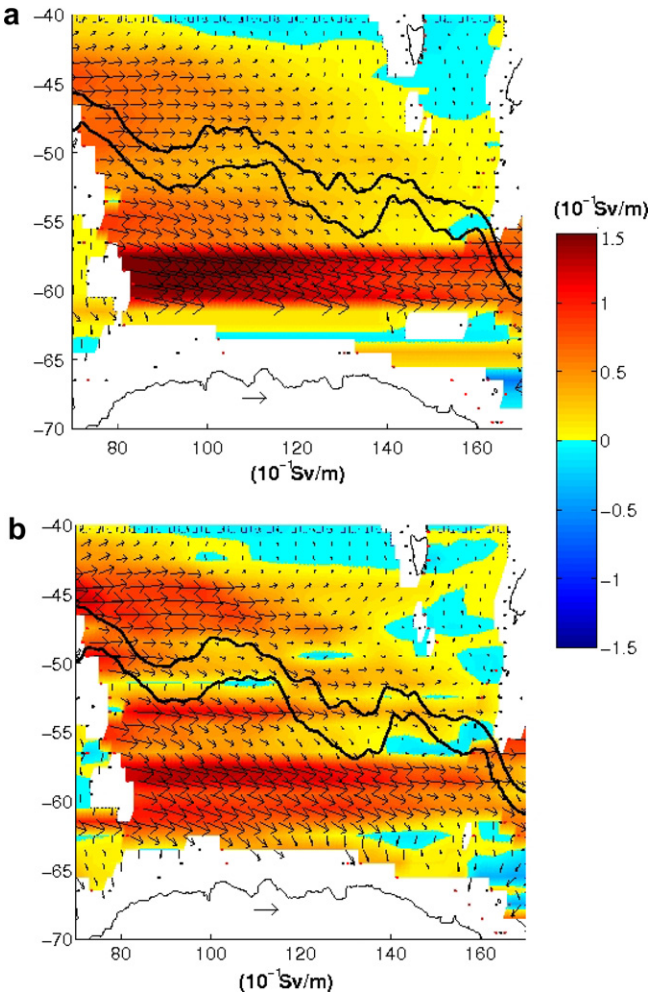

Fig. 13. Sverdrup transport (10^{-4} Sv/m) based on the (a) mean ERS-1 winds (1991–1995) and (b) the mean Quikscat winds (1999–2005), integrated over the Southern Ocean basins deeper than 2000 m. Within each basin, the model integrates wind stress curl from east to west, starting from the 2000 m depth contour along an eastern continental boundary or submarine ridge, up to the western boundary or ridge.

across the SURVOSTRAL line around 47°S. The negative Sverdrup circulation in the SAZ during this period recirculates water from further south in the Tasman Sea, and may contribute to the lower subsurface temperatures in the later years (Figs. 3b and 6) and lower sea level (Figs. 3a and 4a). More strikingly, the cyclonic circulation south of the fronts from 55°S to 65°S has weakened across the whole basin. This implies a reduced transport of cool, fresh water south of the fronts, which is warmer and saltier at depth, which would raise sea level during the early 2000s, as observed (Figs. 5a, 8 and 9).

6. Discussion and conclusion

This study has investigated the causes of the observed sea level rise in the Southern Ocean south of Australia over the 1990s, by examining the vertical temperature structure in the upper ocean from available repeat in situ data.

6.1. Fronts

One clear result of this work is that the position of the main fronts (STF, SAF and PF) show a net shift to the south over the 10

year period. This is despite the fact that the SAF is bounded to the south by the Southeast Indian Ridge. Sallée et al. (2008) have monitored the position of the SAF and PF from 1992 to 2005 using a combination of altimetry and in situ data, and considered the effect of the main climate modes (ENSO, SAM) on the frontal position. In the region south of Tasmania, they find that the SAF is constrained by bathymetry, but the PF shows a net southward shift over the 13 years. Their SAF/PF definition corresponds to the SAF-S/N-PF-S definitions of Sokolov and Rintoul (2002) in the same region. The Sallée et al. (2008) SAF-S and N-PF-S frontal positions are shown in Fig. 3b and c over the period 1992–2005. We can see that during 1992–1996 the fronts were slightly north of their mean position, and during 2000–2004 there is a minor shift to the south. Thus the in situ observations and the altimetry-derived fronts are coherent.

6.2. Salinity in the AZ

Our observations suggest that salinity has decreased in the Winter Water tongue during this decade, although salinity has slightly increased on isopycnal surfaces in the deeper layers. The few subsurface CTD salinity data over the decade and our few spring SURVOSTRAL SSS observations all show a decline in the AASW and WW salinity. In addition, the annual E–P trend follows the summer mean E–P trend (Fig. 5) with increasing precipitation over the decade. The decrease in sea surface salinity in this zone can be explained by the increased precipitation. However, the near constant value of around 33.85 over the 10° latitude band south of the PF is also due to its long advection time. Lagrangian studies of upper ocean currents show that the WW along the SURVOSTRAL line is formed by winter convection in a source region south of 60°S and near 80–100°E. The AASW and WW layers then undergo ~12–18 months of ENE advection before they arrive in the SURVOSTRAL region (i.e. at least one complete seasonal heating/cooling cycle – Speich, S., personal communication). The increase in precipitation at the SURVOSTRAL line (Fig. 5) is also representative of a larger pattern south of the PF in the Indo-Pacific sector (not shown). So the freshening may be related to increased precipitation which occurred along the 12–18 month lagrangian drift (warmer and fresher). We cannot rule out that increased sea ice melt may also contribute to the observed salinity decrease, but that would imply cooler and fresher anomalies. Modelling studies would help to elucidate this point.

6.3. Steric contribution to sea level rise

A trend of increasing XBT temperature in the SAZ is quite coherent over the upper 500 m during the 1990s, with a maximum in temperature increase around 80–150 m and dropping to near zero at 500 m. Assuming a constant salinity of 34.5 over the upper ocean, we have estimated that the steric sea level rise due to these temperature trends in the upper 500 m would account for 1.6 mm/year in sea level rise over the 12 years. This is only 1/3 of the observed sea level rise from the altimeter data (see Fig. 1a), but is in line with recent analyses of global 0–700 m in situ data products (Fig. 1b; Lombard et al., 2005; Ishii et al., 2006). Our CTD sections show that even deeper warming (500–1500 m) may also contribute to the observed sea level rise. The deeper signal may be due to an increased Tasman Sea outflow, bringing warmer, saltier intermediate water across the northern part of the section, which can extend to the sea floor (Rintoul and Sokolov, 2001). Clearly, our XBT sampling to 500 m depth will not be capturing this entire signal.

The Antarctic Zone is where the difference between the altimeter sea level trend and the in situ steric trend is the largest (Fig. 1c). We find distinct changes in the AASW and Winter Water characteristics, as well as deeper warming evident in the CTD sections. The XBT time series show that the surface layer of Antarctic Surface water (AASW) has become warmer and fresher over the last decade. This summer surface mixed layer is shallow, around 55 m ± 10 m (Chaigneau et al., 2004), and so has a limited impact on the observed sea level rise. We estimate that the observed warming by 0.067 °C/year, and freshening by −0.0077 psu/year would contribute to a 0.6 mm/year sea level rise, only a fraction of the observed 4 mm/year sea level rise in Fig. 5a. The subsurface temperature minimum Winter Water layer has also become thinner and shallower, stocking less cold water in the period 2000–2004. The northern limit of the winter water tongue, defined by the PF position, has also shifted south (Fig. 3c). The mean winter water depth from eight years of XBT observations (1992–2000) was 177 ± 11 m (Chaigneau et al., 2004), whereas in the 2000–2004 sections, the Winter Water layer is only 150 m deep (Fig. 8). If we consider that the AASW and the WW layers have decreased in salinity by −0.0077 psu/year, and that the subsurface layers have followed the temperature trends in Fig. 7, then the upper ocean heat and salinity changes would lead to a 1.5 mm/year sea level rise. Our CTD difference plots show a 4 cm rise over the AZ, calculated relative to 2000 dB, over the period to November 2001, roughly equivalent to the 4 mm/year observed with altimetry. Thus it is the deeper changes in the AZ temperature–salinity structure which are mainly contributing to the observed sea level rise.

Our CTD results are only indicative south of Tasmania, since only one recent SR3 CTD section is available. However, the steric height calculated over 0–2000 dB is 2–3 times greater than the 0/500 dB steric height, in the SAZ and the AZ. This suggests that deeper ocean warming below 500–700 m depth can explain the observed altimetric sea level rise, at least south of Tasmania. Part of this warming is clearly associated with the southward frontal movements and water mass redistribution, but whether the water mass characteristics themselves have also changed requires a separate study.

6.4. Response to climate modes

In the AZ, where the SAM forcing dominates, there is a direct relation between the interannual sea level response and the wind stress curl variations. In the SAZ, the interannual variations in sea level rise appear to respond to both the SAM forcing and the negative ENSO (La Nina) events. As the seat of SAMW formation, it is important to understand the relation between the climate forcing and the subsurface water mass characteristics. Unfortunately, it is difficult to extract a subsurface large-scale climate signal from the in situ measurements, when their sampling is dominated by the intense mesoscale eddy field in the SAZ, which itself has strong interannual variability (Morrow et al., 2003). Until we have better subsurface observational coverage (e.g., ARGO), the spatial–temporal variability in the SAZ can only captured by altimetry and numerical models.

Our simple Sverdrup transport model suggests that the vertically integrated wind-driven flow may be partly responsible for the deeper warming trend in the AZ, and may also act to reduce the thickness of the Winter Water tongue. This simple model shows gyre-scale circulation changes, in the right sense to explain the observed sea level rise south of the polar front. Our simple model does not include bathymetry, which is a major constraint in the Southern Ocean, and is also based on two different wind products which may contribute to the differences. More sophisticated models are needed to provide a more precise estimate of the circulation changes over these 15 years.

The CTD sections, and the Sverdrup model results, both underscore how important the deeper ocean changes are in the Southern Ocean, and that calculating sea level trends using only data to

500–700 m will largely underestimate the ocean's response to climate changes.

Acknowledgements

We thank the captain and crew onboard *l'Astrolabe* and the *Aurora Australis*, as well as our numerous volunteer observers, for helping us obtain the in situ measurements in the frequently inhospitable weather conditions. Thanks to Ann Gronell and Mark Rosenberg for their help with quality control of the XBT and CTD data, respectively. We all appreciated the frequent discussions with Kevin Speer during his stay at LEGOS, including his constructive comments on the manuscript. The SURVOSTRAL program receives support from the Institut Polaire – Emile Victor (IPEV) and the Programme Nationale d'Etudes Dynamique du Climat (PNEDC) in France, the Australian Greenhouse Office and the Cooperative Research Centre Program in Australia, and the National Oceanic and Atmospheric Administration (NOAA – USA) through a cooperative agreement NA37GP0518.

References

Belkin, I.M., Gordon, A.L., 1996. Southern Ocean fronts from the Greenwich Meridian to Tasmania. J. Geophys. Res. 101, 3675–3696.

Bindoff, N.L., Rosenberg, M.A., Warner, M.J., 2000. On the circulation and water masses over the Antarctic continental slope and rise between 80 and 150°E. Deep Sea Res. II 47, 2299–2326.

Chaigneau, A., Morrow, R.A., 2001. Surface temperature and salinity variations between Tasmania and Antarctica, 1993–1999. J. Geophys. Res. 107 (C12), 8020. doi:10.1029/2001JC000808.

Chaigneau, A., Morrow, R.A., Rintoul, S.R., 2004. Seasonal and interannual evolution of the mixed layer in the Antarctic Zone south of Tasmania. Deep Sea Res. I 51, 2047–2072.

Cunningham, S.A., Alderson, S.G., King, B.A., Brandon, M.A., 2003. Transport and variability of the Antarctic Circumpolar Current in Drake Passage. J. Geophys. Res. 108 (C5), 8084. doi:10.1029/2001JC001147.

Ducet, N., Le Traon, P.-Y., Reverdin, G., 2000. Global high resolution mapping of ocean circulation from TOPEX/POSEIDON and ERS-1/2. J. Geophys. Res. 105, 19477–19498.

Guinehut, S., Le Traon, P.Y., Larnicol, G., Philipps, S., 2004. Combining Argo and remote-sensing data to estimate the ocean three-dimensional temperature fields – a first approach based on simulated observations. J. Mar. Sys. 46, 85–98.

Hall, A., Visbeck, M., 2002. Synchronous variability in the Southern Hemisphere atmosphere, sea ice and ocean resulting from the annular mode. J. Clim. 15, 3043–3057.

Holbrook, N., Bindoff, N., 1996. Interannual and decadal temperature variability in the Southwest Pacific Ocean between 1955 and 1988. J. Clim. 10 (5), 1035–1049.

Ishii, M., Kimoto, M., Sakamoto, K., Iwasaki, S.-I., 2006. Steric sea level changes estimated from historical ocean subsurface temperature and salinity analyses. J. Oceanogr. 62, 155–170.

Karoly, D., 1989. Southern Hemisphere circulation features associated with El-Nino-Southern Oscillation events. J. Clim. 2, 1239–1252.

Le Traon, P.Y., Dibarboure, G., 1999. Mesoscale mapping capabilities from multiple altimeter missions. J. Atmos. Oceanic Technol. 16, 1208–1223.

L'Heureux, M.L., Thompson, D.W.J., 2006. Observed relationships between the El-Nino/Southern Oscillation and the extratropical zonal-mean circulation. J. Clim. 19 (2), 276–287. doi:10.1175/JCLI3617.1.

Lombard, A., Cazenave, A., Le Traon, P.Y., Ishii, M., 2005. Contribution of thermal expansion to present-day sea level change revisited. Global Planetary Change 47, 1–16.

Morrow, R., Brut, A., Chaigneau, A., 2003. Seasonal and interannual variations of the upper ocean energetics between Tasmania and Antarctica. Deep Sea Res. I 50, 339–356.

Morrow, R., Donguy, J.-R., Chaigneau, A., Rintoul, S.R., 2004. Cold-core anomalies at the Subantarctic Front, south of Tasmania. Deep Sea Res. I 51, 1417–1440.

Nagata, Y., Michida, Y., Umimura, Y., 1988. Variations of positions and structures of the ocean fronts in the Indian Ocean sector of the Southern Ocean in the period from 1965 to 1987. In: Salirhage, D. (Ed.), Antarctic Ocean and Resources Variability. Springer–Verlag, Berlin, pp. 92–98.

Park, Y.H., Gamberoni, L., 1995. Large-scale circulation and its variability in the South Indian Ocean from Topex/POSEIDON altimetry. J. Geophys. Res. 100, 24911–29929.

Reverdin, G., Kestenare, E., Frankignoul, C., Delcroix, T., 2007. Surface salinity in the Atlantic Ocean (30°S–50°N). Prog. Oceanogr. 73(3–4), 311–340.

Reynolds, R.W., Rayner, N.A., Smith, T.M., Stokes, D.C., Wang, W., 2002. An improved in situ and satellite SST analysis for climate. J. Clim. 15, 1609–1625.

Rintoul, S.R., Donguy, J.-R., Roemmich, D.H., 1997. Seasonal evolution of upper ocean thermal structure between Tasmania and Antarctica. Deep Sea Res. I 44, 1185–1202.

Rintoul, S.R., Sokolov, S., 2001. Baroclinic transport variability of the Antarctic Circumpolar Current south of Australia (WOCE repeat section SR3). J. Geophys. Res. 106, 2795–2814.

Rintoul, S.R., Trull, T.W., 2001. Seasonal evolution of the mixed layer in the Subantarctic Zone south of Australia. J. Geophys. Res. 106, 31447–31462.

Roemmich, D., Gilson, J., Davis, R., Sutton, P., Wijffels, S., Riser, S., 2007. Decadal spinup of the South Pacific Subtropical Gyre. J. Phys. Oceanogr. 37, 162–173.

Rosenberg, M.A., Eriksen, R., Bell, S., Bindoff, N. Rintoul, S.R., 1995. *Aurora Australis* marine science cruise AU9407: oceanographic field measurements and analysis. Res. Rep. 6, 97 (Antarctic Coop. Res. Cent., Hobart, Tasmania, Australia).

Sallée, J.B., Morrow, R., Speer, K., 2008. Southern Ocean fronts and their variability to climate modes. J. Clim., in press.

Sokolov, S., Rintoul, S.R., 2002. Structure of Southern Ocean fronts at 140°E. J. Mar. Sys. 37, 151–184.

Sokolov, S., Rintoul, S.R., 2003. Subsurface structure of interannual temperature anomalies in the Australian sector of the Southern Ocean. J. Geophys. Res. 108 (C9), 3285. doi:10.1029/2002JC001494, 2003.

Sokolov, S., Rintoul, S.R., 2007. Multiple jets of the antarctic circumpolar current south of Australia. J. Phys. Oceanogr. 37, 1394–1412.

Speer, K., Forbes, A., 1994. A deep western boundary current in the South Indian Basin. Deep Sea Res. I 41 (9), 1289–1303.

Speer, K., Rintoul, S.R., Sloyan, B., 2000. The diabatic deacon cell. J. Phys. Oceanogr. 30, 3212–3222.

Sprintall, J., 2003. Seasonal and interannual upper-ocean variability in the Drake Passage. J. Mar. Res. 61, 27–57, 200.

Thompson, D., Wallace, J., 2000. Annular modes in the extratropical circulation. Part I. Month-to-month variability. J. Clim. 13, 1000–1016.

Thompson, D.C., Wallace, J., Hegerl, G.C., 2000. Annular modes in the extratropical circulation. Part II. Trends. J. Clim. 13, 1018–1036.

Vivier, F., Kelly, K.A., Harismendy, M., 2005. Causes of large-scale sea level variations in the Southern Ocean: analyses of sea level and a barotropic model. J. Geophys. Res. 110, C09014. doi:10.1029/2004JC002773.

Willis, J.K., Roemmich, D., Cornuelle, B., 2004. Interannual variability in upper-ocean heat content, temperature and thermosteric expansion on global scales. J. Geophys. Res. 109, C12036. doi:10.1029/2003JC002260.

Wong, P.S., Bindoff, N.L., Forbes, A., 1998. Ocean–ice shelf interaction and possible bottom water formation in Prydz Bay, Antarctica. In: Jacobs, S., Weiss, R. (Eds.), Ocean, Ice, and Atmosphere: Interactions at the Antarctic Continental Margin, Antarctic Research Series, vol. 75. American Geophysical Union, Washington, pp. 173–187.

Xie, P., Arkin, P.A., 1997. Global precipitation: a 17-year monthly analysis based on gauge observations, satellite estimates and numerical model outputs. Bull. Am. Meteorol. Soc. 78, 2539–2558.